Catena 200 (2021) 105142

Contents lists available at ScienceDirect

Catena

journal homepage: www.elsevier.com/locate/catena

Geospatial analysis and model development for specific degradation in South Korea using model tree data mining

Woochul Kang [a,*], Eun-kyung Jang [a], Chun-Yao Yang [b], Pierre Y. Julien [c]

[a] Department of Land, Water, and Environment Research, Korea Institute of Civil Engineering and Building Technology (KICT), Goyang-si 10223, Gyeonggi-Do, Republic of Korea
[b] Hydrau-Tech Inc., Fort Collins, CO 80526, United States
[c] Dept. of Civil and Environmental Engineering, Colorado State University, Fort Collins, CO 80523, United States

ARTICLE INFO

Keywords:
Geospatial analysis
Hypsometric analysis
Land use
Model tree
Sediment yield
Specific degradation

ABSTRACT

South Korea experiences numerous local sedimentation problems, such as landslides, upland erosion, aggradation and degradation, and flood plain sediment deposition. This has necessitated the development of a reliable and consistent approach for modeling sediment processes in the country. In this study, samples obtained from 35 gauging stations at five alluvial river basins in South Korea were used together with the modified Einstein procedure and series expansion of the modified Einstein procedure to determine the total sediment load at the sampling locations. Using two different methods, the total sediment load of majority of the 35 considered rivers were found to be typically 50–300 ton/km^2·yr. A model tree data mining technique was used to develop a model for estimating the specific degradation based on certain meaningful parameters, namely, the 1) elevation at the middle relative area of the hypsometric curve [m], 2) percentage of wetland and water, 3) percentage of urban land, 4) mean annual precipitation [mm], 5) main stream length [km], and 6) watershed form factor [km^2/km^2]. The root mean square error of the predictions of the proposed model was found to be 55 ton/km^2·yr less than those of existing statistical models. Erosion loss maps obtained by the revised universal soil loss equation (RUSLE), satellite images, and aerial photographs were also used to represent the geospatial features affecting erosion and sedimentation. The results of the geospatial analysis indicated that the transport of sediment into the alluvial rivers was affected by the wetlands located near the rivers, and also enabled clear delineation of the unique erosion features of construction sites in the urban areas. In addition, the watershed morphometric characteristics could be used to accurately represent the sediment transport. The proposed data mining methodology promises to facilitate the solution of various erosion and sedimentation problems in South Korea. The geospatial analysis procedure would also enable the understanding of spatially varied erosion and sedimentation processes under different conditions.

1. Introduction

South Korea has unique climatic and topographic characteristics with steep mountainous areas and valleys containing wide alluvial plains. Approximately two-thirds of the annual precipitation in the country primarily occurs during the summer season between June and September. The many mountainous areas account for 70% of the total land of the country and the wide alluvial plains between the mountains are used as paddy fields, which account for 13% of the total land area (Lee et al., 2018; Kang et al., 2019; Yoon and Woo, 2000). Thus, the country contains numerous agricultural reservoirs (~17,000) for water resource management. These distinctive conditions complicate sedimentation, resulting in problems, such as upland erosion during typhoons, flood plain sediment deposition, and aggradation and degradation. Additionally, South Korea has experienced rapid urbanization over the last few decades, and some researchers have proposed that human activities affect sediment yield (Knox, 1977; Wessels et al., 2007; Boix-Fayos et al., 2008; Shi et al., 2019;). Hence, there is a need for a reliable and consistent method for predicting sediment yield under the consideration of local conditions (Yoon and Woo, 2000; Kang et al., 2019).

Estimation of the total sediment flux and prediction of the sediment yield are some of the most challenging concerns in the field of erosion and sedimentation. Several methods have been developed for estimating

* Corresponding author.
E-mail addresses: kang@kict.re.kr (W. Kang), jang@kict.re.kr (E.-k. Jang), pierre@engr.colostate.edu (P.Y. Julien).

https://doi.org/10.1016/j.catena.2021.105142
Received 5 March 2020; Received in revised form 25 October 2020; Accepted 31 December 2020
Available online 18 January 2021

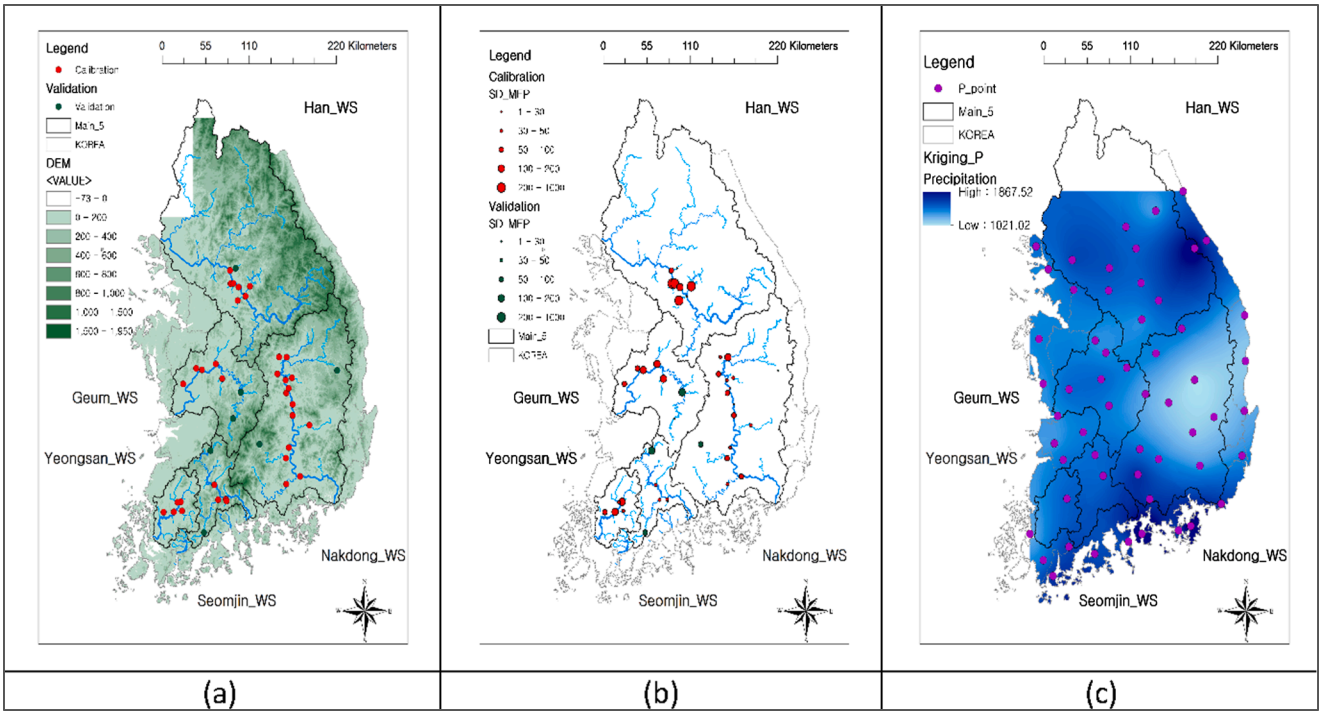

Fig. 1. (a) South Korea and DEM, (b) distribution map of validation and calibration data stations, and (c) precipitation gauging station and kriging result.

the total sediment flux. Einstein (1950) proposed the use of a bed load function for estimating the bed material load in sand beds, and various other studies have been conducted to develop a method to calculate the total sediment load. Colby and Hembree (1955) proposed the modified Einstein procedure (MEP), which can be used to calculate the total sediment bed load through depth-integrated sediment measurements. The Bureau of Reclamation Automated Modified Einstein Procedure (BORAMEP) is a computer program for MEP calculation (Holmquist--johnson, 2006). In 2009, Shah-Fairbank (2009) proposed the series expansion of the modified Einstein procedure (SEMEP) for calculating the total sediment load using depth integration (Yang, 2019; Yang and Julien, 2019). This method produces reasonable results, revealing that the total sediment load is always greater than the suspended sediment load (Julien, 2010). The present study utilized two total sediment discharge values estimated by SEMEP and an MEP-based sediment discharge computation system.

Furthermore, many researchers have developed simulation model for erosion and sedimentation. In particular, various empirical and statistical models have been developed to estimate sediment yield (Langbein and Schumm, 1958; Ryu and Min, 1975; Ryu and Kim, 1976; Allen, 1986; MOC, 1992; Verstraeten and Poesen, 2001; Kane and Julien, 2007; Faran Ali and De Boer, 2008; MLTMA, 2011; Kang et al., 2019). Statistical models generally aim to determine the relationship between the eclectic watershed characteristics and observed sediment (Wheater et al., 1993). Additionally, the universal soil loss equation (USLE), which is an empirical erosion regression equation based on observation, is used worldwide to estimate the average soil loss equation yield (Kim, 2006; Merritt et al., 2003; Shrestha et al., 2004; Gayen et al., 2019). The USLE has been continuously enhanced during the past 50 years by various researchers. Williams (1975) developed the modified universal soil loss equation (MUSLE), which replaced the rainfall factor with a runoff factor in 778 storm runoff events in 18 watersheds. The

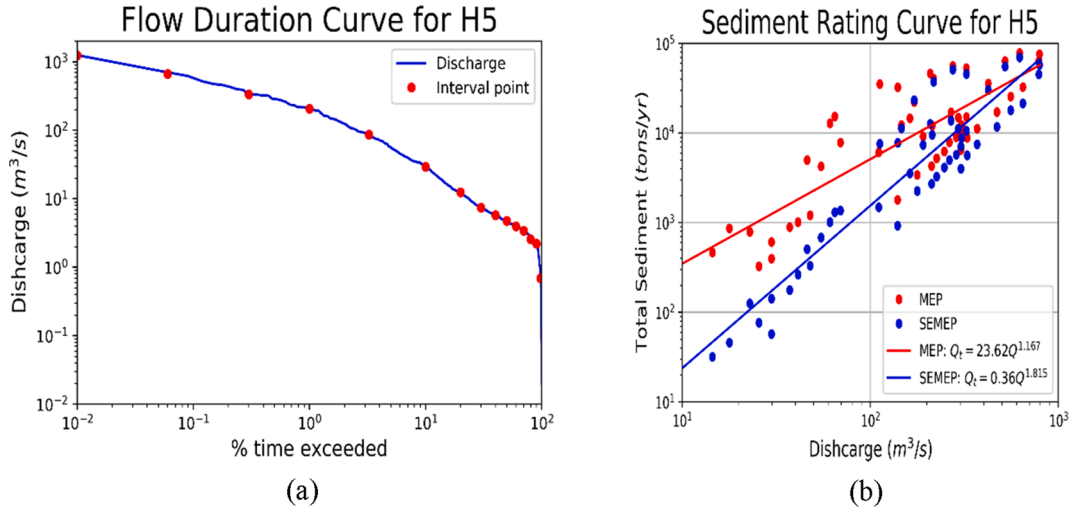

Fig. 2. (a) Flood duration curve and (b) sediment rating curves (MEP and SEMEP) for station H5.

Table 1
Variables considered in empirical model.

Category	Variables
Watershed morphometric	Line: total, main, tributary stream length, three stream orders Area: watershed area, drainage density, length factor, shape factor Relief: average watershed slope, river slope, middle relative height at middle relative area, elevation at middle relative area, lowest elevation, middle elevation, and hypsometric index
Precipitation	Precipitation at gauging station and in basin area, rainfall erosivities at gauging station in basin area
Land cover	Percentages of urban land, agricultural land, forest, pastoral land, bare land, wetland, water area, and wetland and water area
Soil type	Sand, clay, silt, and rock at 0–10 cm effective soil depth
Bed material	Minimum and maximum size of bed material

revised universal soil loss equation (RUSLE) upgraded the USLE by focusing on better parameter estimation (Renard et al., 1997). However, because the empirical and statistical models are based on different conditions, they often produce highly variable results. To predict the sediment yield using statistical and empirical models, priority should be given to careful selection of the considered factors and proper understanding of their influence mechanisms. The reliability of the model output should also be carefully investigated (Vente et al., 2011).

Recently, several data-based methods have been proposed for systematically and automatically deriving statistical rules and patterns from big data composed of various variables. The most representative prediction and classification analysis techniques for data mining include artificial neural network (ANN), regression analysis, logistic regression analysis (LRA), and decision tree. Data mining techniques have also been used to determine the correlations between input and output variables, as well as in identifying rules or trends based on the characteristics of the data. Several studies have adopted data mining to develop calculation methods that consider various variables, derive new empirical equations, and make predictions based on the correlations between data (Chen et al., 2017). Additionally, several attempts have been made to model hydraulic sediment transport using machine learning (Bhattacharya et al., 2007), genetic programming (Iovine et al., 2005; Aytek and Kişi, 2008), gene expression programming (Ebtehaj et al., 2015; Ghani and Azamathulla, 2011), ANNs (Jain, 2001; Lin and Namin, 2005; Nagy et al., 2002; Zhu et al., 2007), and adaptive neural fuzzy technology (Cobaner et al., 2009; Ostovari et al., 2016; Viloria et al., 2016). Therefore, data mining may be considered as a suitable method for estimating sediment discharge based on the strong correlations between several physical quantities. In this study, data mining model tree techniques were used to develop models for predicting the mean annual specific degradation. The developed models were validated using additional data and the predictions were compared with those of existing models. Additionally, geospatial analysis using erosion maps obtained by RUSLE, satellite images, and aerial photographs was used to evaluate the reliability of the meaningful parameters employed in the proposed models.

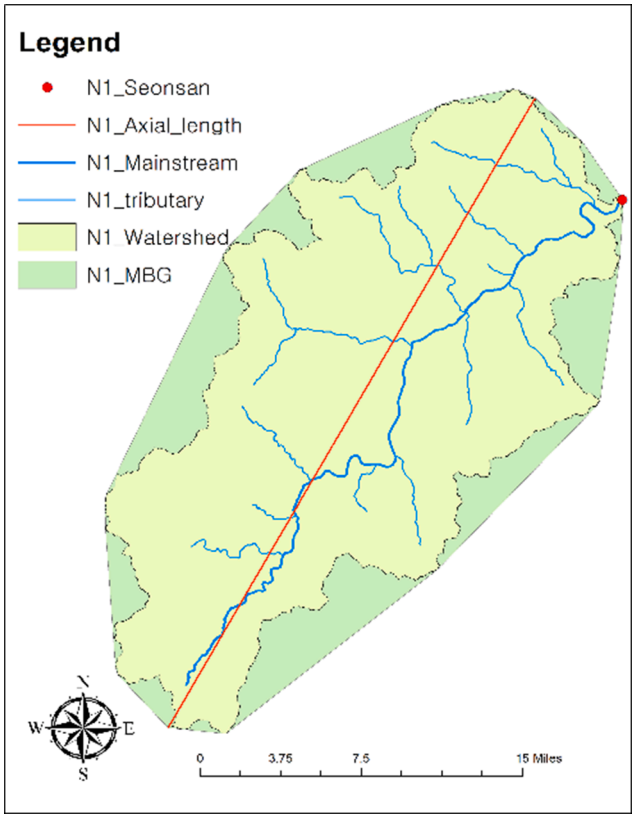

Fig. 3. Watershed length for aerial morphometric characteristics (shape and form factors) and watershed length, *MBG is minimum bounding geometry.

2. Materials and methods

As mentioned in the introduction, South Korea has distinctive climatic and topographic characteristics. The mountainous Korean Peninsula includes an eastern region of high mountain ranges and a narrow coastal plain, and western and southern regions containing coastal plains, relatively wide alluvial river basins, and rolling hills (Fig. 1a). There are five main rivers in South Korea (Han, Nakdong, Geum, Yeongsan, and Seomjin rivers), with all of them flowing from east to west, except the Nakdong river (Fig. 1b). Because the Korean Peninsula is affected by the East Asia monsoon, rainfall occurs mainly in summer during the rainy season. Fig. 1b illustrates the distribution of mean annual precipitation over 30 years. The large variation in the river flow under climatic and topographic conditions causes sediment problems in river management. This study considered 35 gauging stations in five major rivers in the alluvial river basin and analyzed the daily discharge data over 10 years. Most rivers in South Korea are alluvial sand bed rivers, and the gauging stations used for calibration in this study were almost within the transfer zone, which is relatively stable (Woo et al., 2015). In this zone, streams merge and flow down mild slopes, transporting water and sediment along the river bed. Because most of the sediment measurements in this study were performed during flooding, the sediments were predominantly suspended in transport. A total of 2084 suspended sediment measurements were performed at the stations, as depicted in Fig. 1a and b. Among these measurements, 2036 measurements were conducted using a depth-integrating method with a D-74 sampler. The remaining measurements were conducted using a surface sampler or a P-61 sampler. The total sediment discharge was calculated using MEP and SEMEP, respectively. As the sediment measurement does not cover the entire water column, the accurate estimation of the total sediment discharge is dependent on the measured concentration and the samples may be representative of concentrations near the bed. The Rouse (1937) suggested an equilibrium concentration profile and the original Einstein procedure assumed that the Rouse number (R_0) varied empirically. The MEP used in this study is similar with the BORAMEP and the R_0 should be determined based on the power relation $R_0 = \alpha\omega^{\beta}$, in this method (where, ω is the settling velocity; α and β are determined by calibration). This method requires at least two overlapping bins between the bed load and the suspended load to calculate the vertical distribution of the sediment (Shah-Fairbank, 2009). In the SEMEP, R_0 was directly calculated from the median grain size of the suspended material to avoid unrealistic results and significant errors as in the overlapping bin approach. In this study, a total of 1962

Table 2
Existing statistical models for predicting sediment yield.

Author *Abbreviation	Model	No. of sediment samples	Location
Langbein and Schumm (1958) *LS58	$SD = 10P^{2.3}/1 + 0.0007P^{3.33}$ (P in inch and SD in ton/mi^2·yr)	170	US (Global)
Allen (1986) *A86	$SD = 2.81{*}D + 1.81$;	17	
Kane and Julien (2007) *KJ07	$SD = 0.02P^{1.7}e^{-0.0017P}SD = 410A^{-0.009}$	488	
Verstraeten and Poesen (2001) *VP01	$SD = 25A^{-0.4}\ln SD = 3.72 - 0.72lnA - 0.84lnHI + 0.11lnTL$ (A in ha and SD in ton/ha·yr)	26	Belgium (Global)
Faran Ali and De Boer (2008) *FD08	SD $= -8867 + 9.72$P; lower, monsoon subbasin	14 3	India (Global)
Ryu and Kim (1976) *RK76	$V_r = 672.61P^{0.024}V_r = 267.21S^{0.587}$	9 9 9	
KICT (1992) *KICT1992	$SD = 972D^{1.039}M^{-0.825}$; for $200 < A < 2000$ $SD = 8668A^{-0.896}$; for $A < 200$	8	
Yoon (2011) *Y2011	$V_r = 43,954 \times A^{0.464}S^{-2.00}M^{-0.855}$	10	
Kang et al., (2019) *K2019	$SD = 357.16A^{-0.204}SD = 3.35 \times 10^{-7}A^{-0.16}P^{2.864}SD = 0.0003 \times A^{-0.08}P^{1.65}U^{0.75}SD = 1.75 \times 10^{-7}A^{-0.05}P^{1.89}U^{0.89}Sa^{1.931}SD = 1.77 \times 10^{-5}A^{-0.009}P^{1.91}U^{0.53}Sa^{1.09}S^{-0.93}SD = 2.45 \times 10^{-7}A^{-0.04}P^{1.94}U^{0.61}W^{-0.64}Sa^{1.51}Hyp^{1.84}$	29	

A: watershed area (km^2), D: drainage density (km/km^2), HI: hypsometric integral (H_{mean} - H_{min}/H_{max} -H_{min}), M: bed material size (mm), P: mean annual precipitation, R: basin relief (H_{max} - H_{min}) (J/ha), S: average watershed slope (%), Sa: percentage of sand (%), SD: specific degradation (ton/km^2·yr), Sl: river slope (%), S_f: watershed shape factor, TL: total stream length (m), V_r: specific sediment deposit (m^3/km^2·yr).
* Abbreviation is used in Fig. 5 and Table 6.

sediment measurements were used for the MEP and 1808 samples were used for the SEMEP. The detailed processes of the SEMEP method are available in Yang and Julien (2019). The annual total sediment load was estimated using the flow duration–sediment rating curve (FD-SRC) method. The flow duration curve was delineated by the Weibull method, which was used to estimate the exceedance probability from the 10-year daily discharge data. The results for station H5 (Cheongmi) are depicted in Fig. 2a, while the corresponding sediment rating curve is depicted in Fig. 2b. From the discrete values of the discharge (red points in Fig. 2, determined empirically based on Julien's method) and the corresponding total sediment loads on the sediment rating curve, the average annual sediment load was estimated. Because the discharge records are available for longer periods than sediment records, this method enables the expansion of a small amount of total sediment yield data to the longer period of flow (Sheppard 1965). The specific degradation was determined as the average annual sediment yield divided by the watershed area. Detailed descriptions of the data processing are provided by Julien (2010) and Kang et al. (2019).

Thirty-two parameters were considered as explanatory variables and classified into five categories, as detailed in Table 1.

These parameters are often used for sediment yield and watershed hydrology modeling. The initial focus of the present study was the morphometric characteristics of the watershed. The relevant parameters were estimated during the watershed delineation using a 5-m discrete element model (DEM), provided by the National Geographic Information Institute. The linear watershed parameters included those that defined the stream network and order. The stream network was delineated using the Korea Reach File (KRF) version 3 as a polygon line, provided by the Ministry of Environment. After the delineation, the common two-dimensional watershed characteristics related to the watershed shape, such as the watershed area, drainage density, form factor, and shape factor, were determined.

$$\textbf{Shape factor} = \textit{Watershed length}^2/\textit{Watershed area} \quad (1)$$

$$\textbf{Form factor} = \textit{Watershed area}/\textit{Watershed length}^2 \quad (2)$$

The form factor represents the ratio of the watershed area to the square of the watershed length. The watershed length can be defined in different ways (see Fig. 3). In this study, the watershed length was considered as the axial length, which is the length of the longest straight line between any two points on the watershed perimeter (red line in Fig. 3). Conversely, the main stream length (blue line in Fig. 3) was used to calculate the shape factor (Horton, 1932; Horton, 1945; Singh, 1994). The form and shape factors are commonly used to explain the surface runoff flow and effectively evaluate the shape of the watershed (perpendicular or circular). If a watershed is long and narrow, a longer time would be required for water and sediment to travel between its extremities. The relief factors of the watershed morphometry are the most important variables for describing the watershed topography. The basin hypsometry is particularly related to the flood response, soil erosion, and sedimentation process (Langbein, 1947; Strahler, 1952). A simple mathematical equation (middle elevation – lowest elevation)/(highest elevation – middle elevation) is often used to express the integral of the hypsometric curve (Özkaymak and Sözbilir, 2012). In this study, a 5-m DEM was used for reclassification at every 100 m, and the reclassification raster was then normalized to draw the hypsometric curve. With the aid of the hypsometric curve, the relative height and elevation at the middle relative area were used to explain the specific degradation. Raindrops were observed to affect the soil detachment, and the surface flow of the precipitation contributed to sediment transportation. The raster result of the kriging was applied to 60 points of daily precipitation and the rainfall erosivity data obtained from the Korea Meteorological Administration (KMA). The rainfall erosivity was calculated by

$$R = \sum E \cdot I_{30}, E = \sum e \cdot \Delta P, e = 0.29[1 - 0.72\exp(-0.05 \cdot I)] \quad (3)$$

where R is the rainfall erosivity factor (10^7 J/ha▪mm▪h), I_{30} is the maximum 30-min rainfall intensity (mm/h), E is the total storm kinetic energy (10^7 J/ha), ΔP is the increase in rainfall in the duration of rainfall interval (mm), e is the estimated unit rainfall kinetic energy (MJ/ha▪mm), and I is the rainfall intensity (mm/h). The first step of kriging is

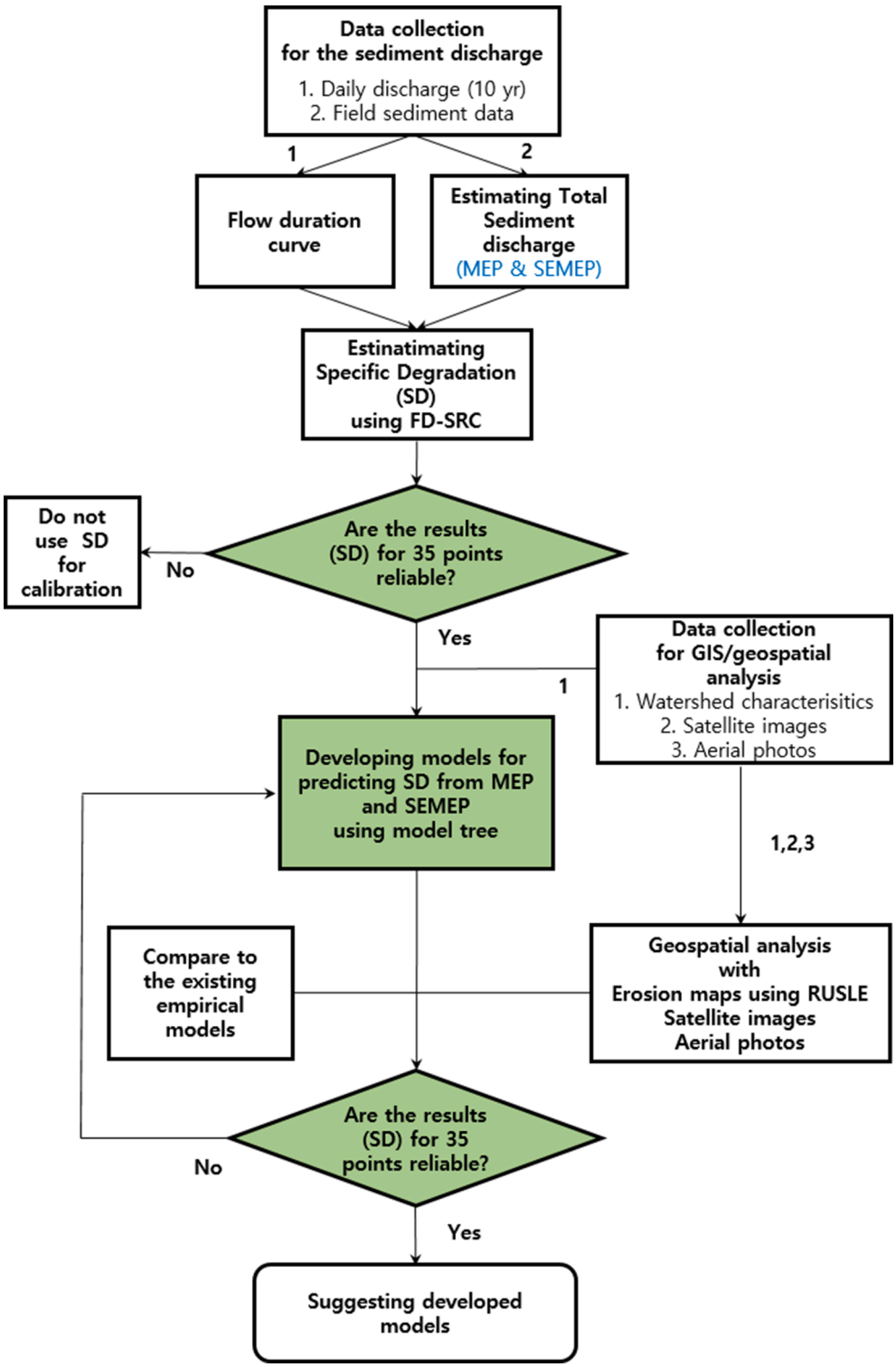

Fig. 4. Flow chart of this study.

model fitting and the next step is prediction. The ordinary kriging with the exponential semivariogram model is highly reliable for most data set and it was used for the fitting of rainfall data (ESRI, 2020). The continuous raster data at a 5-m resolution were created using the fitted model and spatial information (Fig. 1c). This geostatistical method can determine the spatial distribution of meteorological data (Ozturk and Kilic, 2016)

A detailed soil map was generated from the 5-m raster data obtained from the National Institute of Agricultural Sciences and was used to estimate the soil type percentages. The specific information of the percentage of soil and rock was exported from the data of a semi distributed hydrologic model, SWAT-K, developed from the Korea Institute of Construction Technology (KICT, 2007). The soil types were classified as (1) clay ($d_{clay} \leq 0.002$ mm), (2) silt ($0.002 < d_{silt} \leq 0.05$ mm), (3) sand ($0.05 < d_{sand} \leq 2$ mm), and (4) rock ($2\text{ mm} < d_{rock}$) at effective soil depths of 0–10 cm. Here, d denotes the grain size of each soil type for classification. Because land use also impacts soil erosion and sedimentation, the land cover raster (5 m resolution) of the Ministry of

Table 3
Annual sediment load and specific degradation determined by MEP and SEMEP, respectively.

Station no.	Station name	Area	MEP		SEMEP	
			Annual sediment load	Specific degradation	Annual sediment load	Specific degradation
		[km^2]	[ton/yr]	[ton/km^2·yr]	[ton/yr]	[ton/km^2·yr]
H1	Yeoju	11,047	1,295,000	117	755,000	68
H2	Heungcheon	284	114,000	404	126,000	443
*H3	Munmak	1346	1,543,000	1147	317,000	236
H4	Yulgeuk	173	35,000	203	47,000	271
H5	Cheongmi	519	214,000	412	94,000	182
H6	Namhanriver	8823	207,000	24	192,000	22
H7	Heukcheon	307	23,000	75	30,000	97
N1	Seonsan	979	69,000	71	44,000	45
N2	Dongchon	1541	67,000	43	46,000	30
N3	Gumi	10,913	229,000	21	201,000	18
N4	Nakdong	9407	413,000	44	387,000	41
N5	Waegwan	11,101	622,000	56	518,000	47
N6	Ilseon bridge	9533	39,000	4	45,000	5
N7	Jindong	20,381	2,087,000	102	1,031,000	51
N8	Jeongam	2999	100,000	33	88,000	29
N9	Hyangseok	1512	127,000	84	84,000	56
N10	Dongmun	175	13,000	75	7,000	40
N11	Jeomchon	615	24,000	39	22,000	36
N12	Yonggok	1318	61,000	46	35,000	27
N13	Jukgo	1239	46,000	37	64,000	52
N14	Gaejin2	750	39,000	52	31,000	42
G1	Hoedeok	606	72,000	119	60,000	98
G2	Gongju	6275	682,000	109	499,000	80
G3	Hapgang	1850	247,000	134	211,000	114
G4	Useong	258	16,000	61	13,000	49
G5	Guryong	208	12,000	60	14,000	67
Y1	Hakgyo	190	19,000	97	16,000	82
Y2	Naju	2039	233,000	114	190,000	93
Y3	Mareuk	668	111,000	166	97,000	145
Y4	Nampyeong	580	27,000	47	22,000	38
Y5	Seonam	552	22,000	40	17,000	30
S1	Jukgok	1269	41,000	32	42,000	33
S2	Gokseong	1788	80,000	45	84,000	47
S3	Gurye2	3818	172,000	71	138,000	36
S4	Yongseo	128	4000	28	4000	29

* Station is not used for calibration.

Environment was used to estimate the land use ratios in the watershed. This raster includes medium scale classification (22 categories) for land cover at a 5 m resolution. The land cover was classified using the hybrid method, which is a combination of the unsupervised and supervised method, from the Landsat TM, IRS 1C, SPOT5, and Arirang satellite images (Me, 2002). The land cover raster was reclassified into seven simplified categories, namely, 1) urban land, 2) agricultural land, 3) forest, 4) wetland, 5) pastoral land, 6) bare land, and 7) water. The percentages of wetland and water were introduced as additional land use parameters. Other variables related to the bad material size were also employed, and were classified as minimum and maximum bad material sizes based on the d_{50} values before and after flood events. The detailed process and data information are available in Kang (2019).

Model tree is a representative and simple prediction and classification method in data mining, and is known to be the best approach for interpreting results obtained for an enormous amount of various types of data. In particular, model tree is a simple yet excellent technique that can effectively derive explicit formulas, such as empirical formulas. This

Table 4
Specific degradation models developed by MEP and SEMEP.

Conditions				Model (MEP)
Hyp [m]	Main [km]	WW [%]	U [%]	
≤187	–	–	–	$M1 = 661 \times U^{0.55} \times WW^{-0.34} \times hyp^{-0.44}$
> 187	≤265	≤2.63	≤3.11	$M2 = 109 \times U^{0.63} \times WW^{-0.26} \times hyp^{-0.23}$
			> 3.11	$M3 = 112 \times U^{0.64} \times WW^{-0.26} \times hyp^{-0.23}$
		> 2.63	–	$M4 = 113 \times U^{0.58} \times WW^{-0.27} \times hyp^{-0.23}$
	> 265	–	–	$M5 = 101 \times U^{0.56} \times WW^{-0.18} \times hyp^{-0.23}$
Conditions				Model (SEMEP)
Hyp [m]	P [mm]	FF [–]	U [%]	
≤187	–	–	–	$M1 = 4.9 \times 10^{-4} \times P^{1.89} \times U^{0.38} \times hyp^{-0.39}$
> 187	≤1133	–	–	$M2 = 3.2 \times 10^{-5} \times P^{2.05} \times U^{0.39} \times hyp^{-0.21}$
	>1133	≤0.33	–	$M3 = 8.3 \times 10^{-4} \times P^{1.61} \times U^{0.41} \times hyp^{-0.21}$
		> 0.33	≤2.61	$M4 = 8.5 \times 10^{-4} \times P^{1.61} \times U^{0.43} \times hyp^{-0.21}$
			>2.61	$M5 = 8.7 \times 10^{-4} \times P^{1.61} \times U^{0.43} \times hyp^{-0.21}$

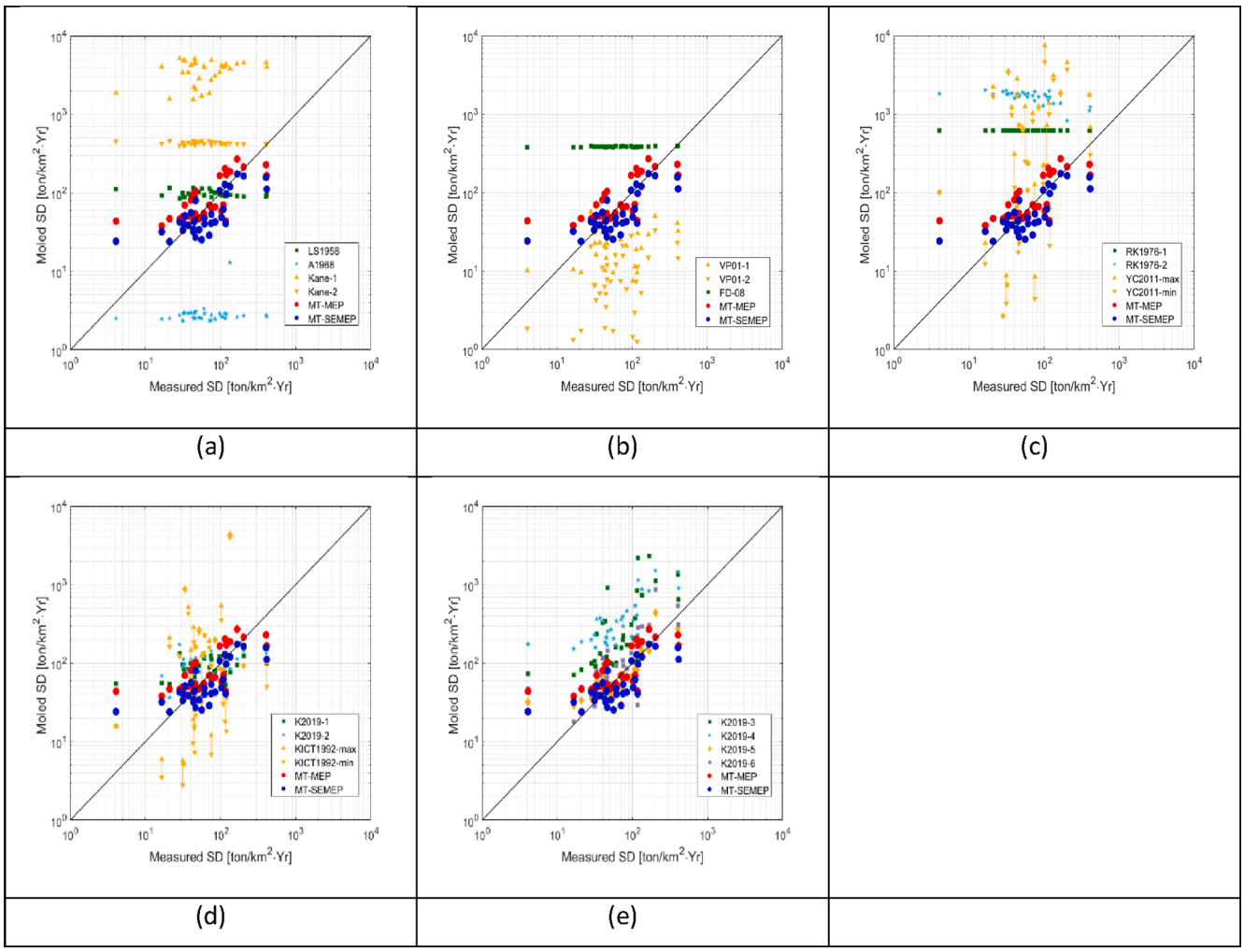

Fig. 5. Validation of existing specific degradation models: (a) US models, (b) global models, (c) Korean model based on reservoir, (d) Korean model with 1 and 2 variables, and (e) Korean model with many variables, * MT_MEP is the suggested model using the model tree and MEP and MT_SEMEP is the proposed model using the model tree and SEMEP.

Table 5
Validation dataset.

Name	Main [km]	P [mm]	FF [%]	U [%]	WW [%]	Hyp [m]	SD [tons/km^2■yr]	Reference
Cheongsong	99	1074	5.32	1.40	1.83	455	24	
Geochang1	71	1309	2.69	1.94	0.48	639	99	
Oesong	401	1523	4.30	2.84	1.66	530	104	
Hotan	394	1267	9.25	2.21	2.31	417	18	
Gwanchon	162	1335	4.99	2.54	2.34	413	120	
Gyeombaek	118	1434	6.11	3.04	1.97	265	56	
Hwajeon Bridge	27	1407	0.45	3.46	0.19	516	136	KICT (1992)
Daeso Bridge	67	1279	0.22	2.51	0.32	348	107	

Table 6
Results of the statistical validation of existing models (MT: model tree).

		FD08	VP01-1	YC11	K2019 −5	K2019 −6	MT MEP	MT SEMEP
MEP	RMSE	3797	112	1242	80	76	67	69
	MAPE	7645	83	1087	113	54	50	52
	NSE	−2066	−0.80	−220	0.09	0.17	0.32	0.31
SEMEP	RMSE	3809	96	1245	73	62	55	53
	MAPE	8283	81	1336	128	63	43	41
	NSE	−2541	−0.63	−230	0.07	0.33	0.47	0.48

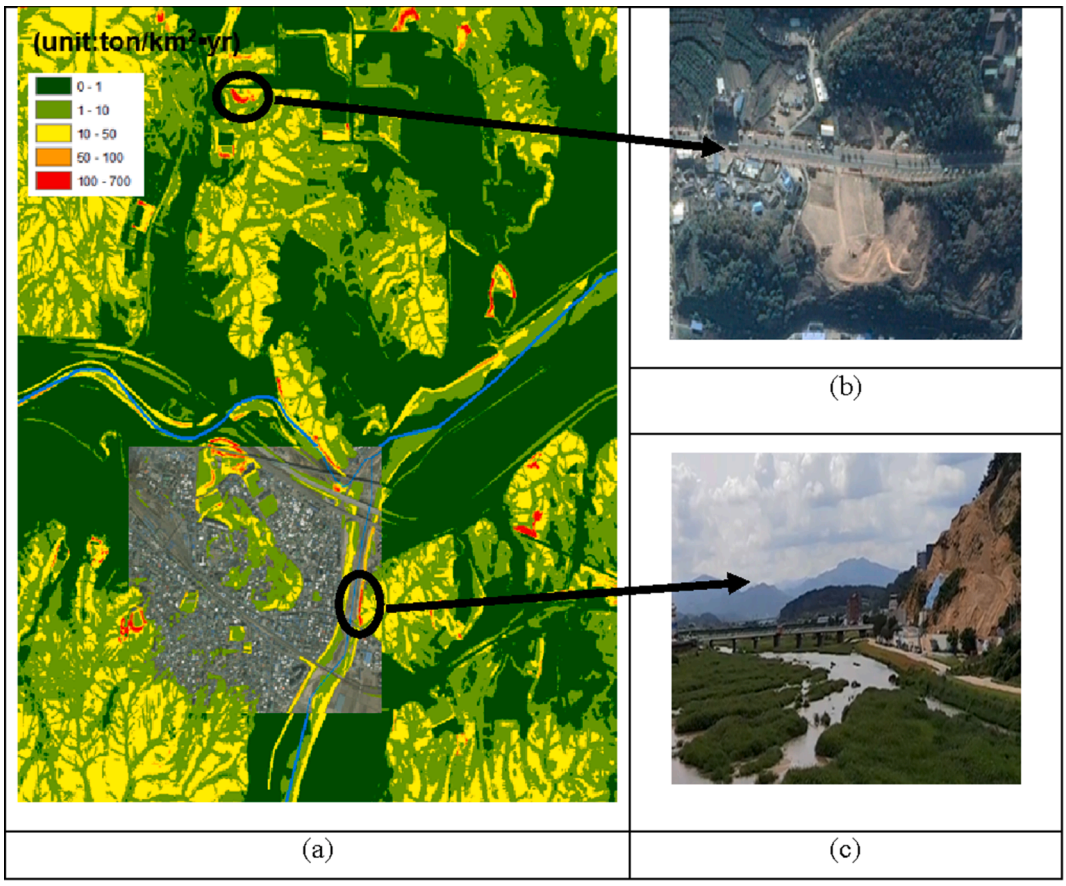

Fig. 6. Results of the geospatial analysis of the urban land at station N1: (a) erosion map, (b) satellite image, and (c) aerial photograph.

technique is considered the most suitable for calculating the SD wherein several sediment physical quantities are transported in complicated connections with each other. The model tree is based on the separation of data into subtrees, which become more homogeneous in terms of the dependent variables, resulting in good predictions or classification rules. The model tree process consists of growing, pruning, and smoothing when the standard deviation reduction of Eq. (4) reaches its maximum value, and is then transferred from a large branch to a small branch (Quinlan, 1992; Wang and Witten, 1996).

$$\begin{matrix}\textit{Standard deviation}\\ \textit{reduction}\end{matrix} = \sigma(\mathrm{T}) - \sum_i \frac{|T_i|}{|T|} \times \sigma(T_i) \tag{4}$$

where T is the set of total samples of the dependent variable, T_i is the set of subsamples of the dependent variable divided by the sub-intervals, σ is the standard deviation, and |T| and $\lceil T_i \rceil$ are the sets expressed by the number of elements. Each independent variable's grouping is determined by the standard deviation reduction rate of the dependent variable. After calculating the standard deviation $\sigma(\mathrm{T})$ from the entire sample set T, including unnecessary branches, it is divided into arbitrary sub-sections according to the random intervals for each independent variable. Among the randomly divided sub-sections, the section with the most considerable standard deviation reduction rate is selected and replaced, after which the lower tree is established. The growth of the tree is terminated when the standard deviation reduction rate reaches the desired value, or when the number of data remaining after grouping becomes smaller than the selected criteria. In this study, the minimum data under the model tree classification conditions were set to four. The standard deviation reduction was set to 5% because an excessively small value would lead to unnecessarily numerous trees, resulting in reduced stability of the new formula. In other words, if the standard deviation reduction does not decrease by more than 5% even after classification, the growth of the tree would be terminated. After the completion of all classification processes, a representative formula of data belonging to the same group is presented through multiple regression analysis. In this study, a model tree that affected sediment formation and transport and watershed characteristic factors were applied to analyze a large amount of sediment data measured in the field, and an SD calculation model for each watershed was attempted. One of this technique's advantages is that it creates a homogeneous data group through subgroups within a group of data without specific rules or uniformity and presents an optimal multiple regression equation through this process (Jang, 2017).

Table 2 enumerates various existing empirical equations of the sediment yield and specific degradation. The existing models are referenced for the selection of appropriate variables. Additionally, the proposed models using the model tree were determined to compare their prediction accuracies with those of the existing models.

The root mean square errors (RMSEs), mean absolute percent errors (MAPEs), and Nash–Sutcliffe efficiency (NSE) coefficients of the models were determined using eight additional validation data to evaluate their prediction accuracies. The NSE varies from −∞ to 1, and it indicates that the model predictions well match the observations when it is close to 1.

$$\mathbf{RMSE} = \sqrt{\frac{1}{\mathbf{n}} \sum_{\mathbf{i}=1}^{\mathbf{n}} (\mathbf{x_i} - \mathbf{y_i})^2} \tag{5}$$

$$\mathbf{MAPE} = \frac{1}{\mathbf{n}} \sum_{\mathbf{i}=1}^{\mathbf{n}} \frac{|\mathbf{x_i} - \mathbf{y_i}|}{\mathbf{x_i}} \times 100 \tag{6}$$

$$\mathbf{NSE} = 1 - \frac{\sum_{\mathbf{t}=1}^{\mathbf{n}} (\mathbf{x_i} - \mathbf{y_i})^2}{\sum_{\mathbf{t}=1}^{\mathbf{n}} (\mathbf{x_i} - \bar{\mathbf{x}})^2} \tag{7}$$

where x_i is the observation value, y_i is the forecast value and $\bar{x}$ is average

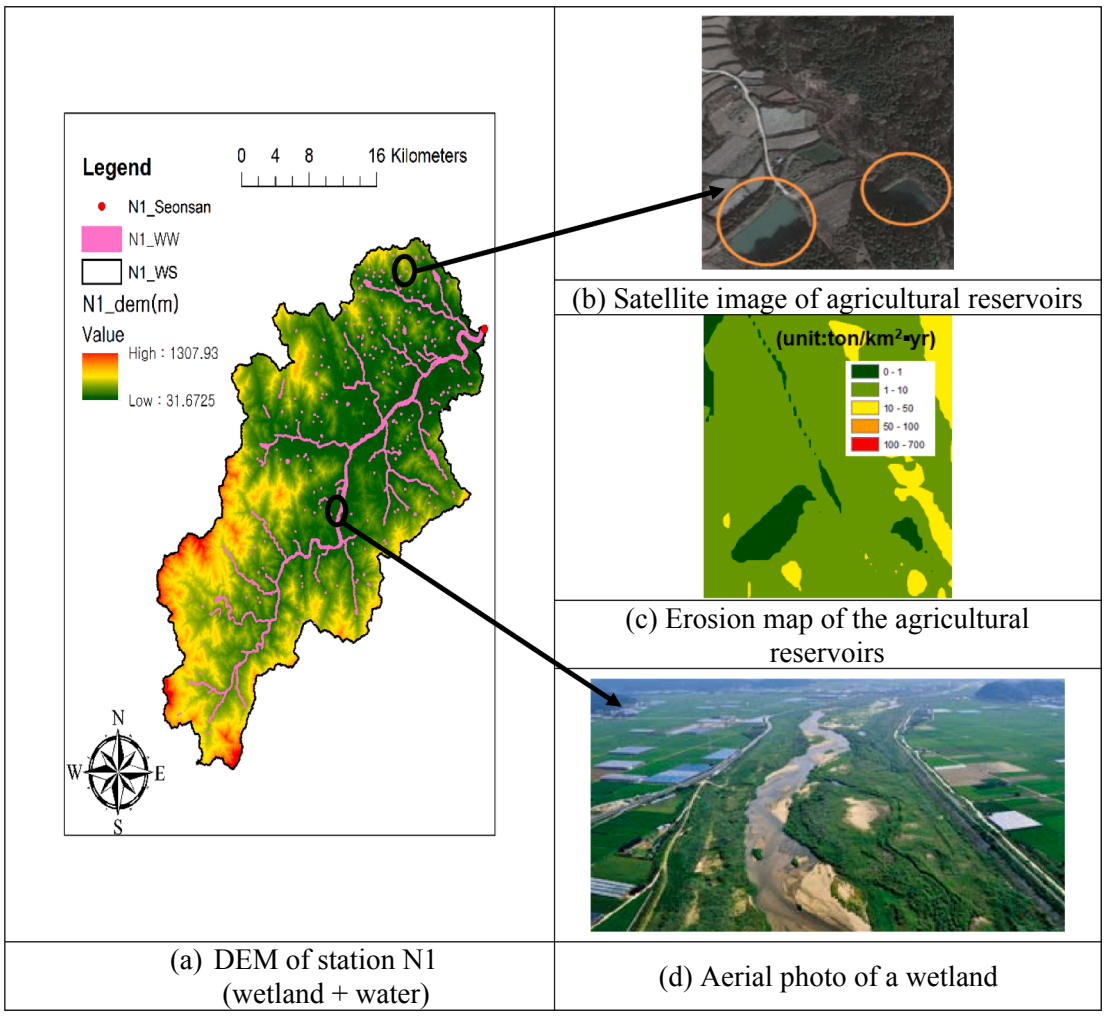

Fig. 7. Locations and geospatial analyses at station N1: (a) DEM and location of a wetland and water area, (b) satellite image of agricultural reservoirs, (c) erosion map of the agricultural reservoirs, and (d) aerial photo of a wetland.

of the observation values.

Finally, the geospatial analysis for upland erosion was conducted with erosion maps using the revised universal soil loss equation, satellite image, and aerial photo. The RUSLE model for the estimation of the average annual soil loss (A) was developed based on five factors: (1) rainfall erosivity factor (R); (2) soil erodibility factor (K); (3) slope length and steepness factor (LS); (4) cover management factor (C); (5) conservation practice factor (P). In this study, the erosion map at a 5-m resolution was created as below. Wischmeier's equation was used for calculating the soil erodilibility factor for each great soil group (Wischmeier et al., 1971). The most sensitive factor in the RUSLE is the slope length and steepness factor, which was estimated using Van Remortel, Hamilton and Hickey's method (Van Remortel et al., 2001). This method could avoid overextensions under the consideration of the downhill slope angle and non-cumulative slope length. The cropping management factor and conservation practice factor were referenced from the Ministry of Environment's regulation (ME, 2012). The generated erosion map had a 5-m resolution. The erosion mapping using the RUSLE was conducted to estimate the overall sediment budget and identify meaningful erosional and sediment features. Then, a geospatial analysis was performed through a comparison of the proposed model calculation with satellite images and aerial photos. A flowchart of the entire process in this study is illustrated in Fig. 4. The results of the specific degradation calculation and the development of models for specific degradation are presented in the third section. Furthermore, the evaluation of the proposed model using geospatial analysis and physiographical analysis is discussed in the Discussion section.

3. Results

The annual sediment load estimated by MEP and SEMEP for the different gauging stations are shown in Fig. 1 and the specific degradation determined by MEP and SEMEP are presented in Table 3. The specific degradations estimated by MEP were slightly higher than those obtained by SEMEP and this is similar with the results reported in another paper (Julien, 2010). Because H3 has the highest difference and the result is unreasonable, H3 stations were discarded from the model tree analysis.

The mean annual specific degradation determined by MEP and SEMEP were adopted as response variables and the model tree data mining process was used to develop a sediment yield model using the above-mentioned 32 parameters as the dependent variables (Table 4).

Each of the two developed models had five versions, all of which incorporated the elevation in the middle relative area and the percentage of urban land. Other meaningful parameters suggested for the MEP model were the main stream length and percentages of wetland and water, while those suggested for the SEMEP model were the mean annual precipitation and form factor. In Fig. 5, the existing models are classified into Global and Korea model based on their study area and they are validated with 8 additional validation data (Table 5).

When the models include bed material size, two results are provided with the minimum and maximum of bed material size. Other regression

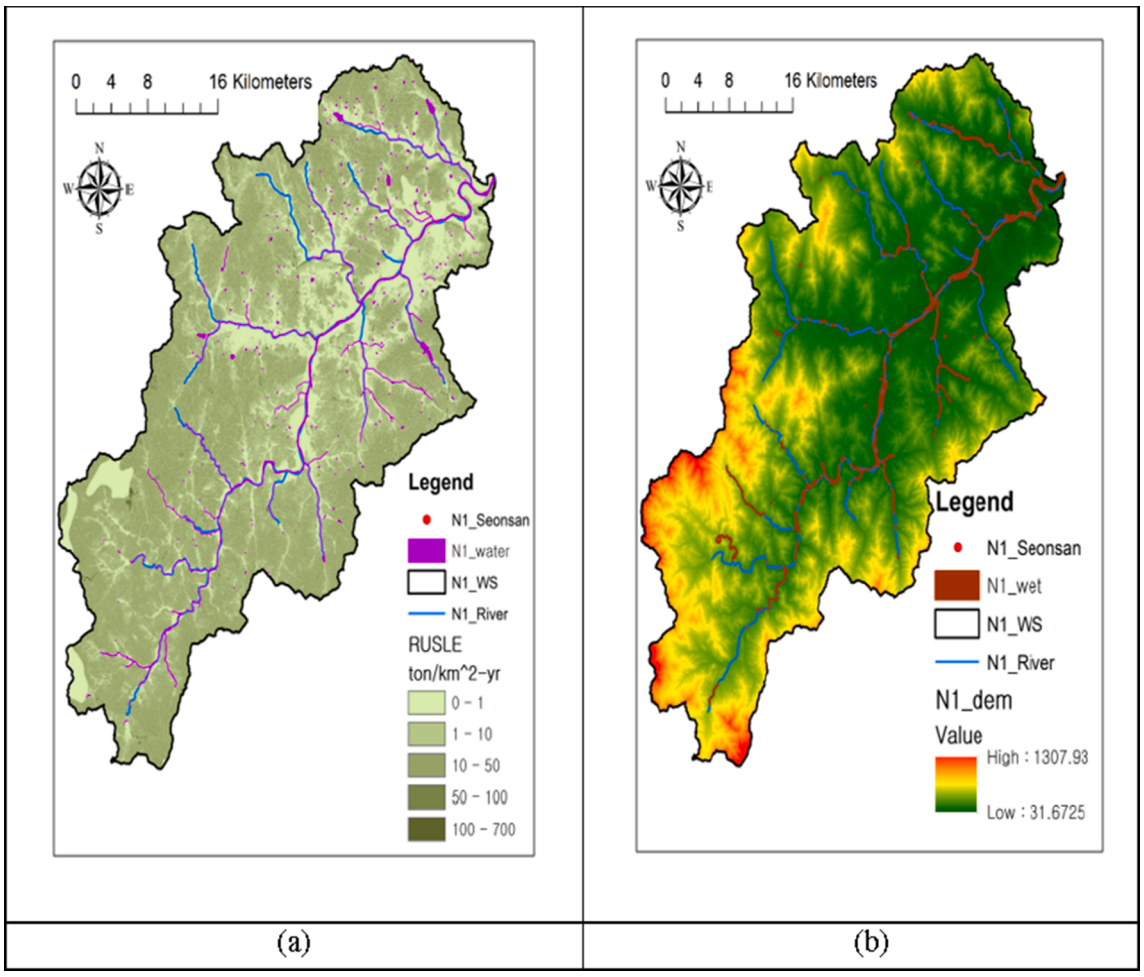

Fig. 8. (a) Erosion map of station N1 and (b) DEM and locations of wetlands and water areas.

models were validated with eight additional validation data (Table 6) and models based on small areas in South Korea were also found to be incapable of representing the sediment yield in other regions.

The results presented in Table 6 reveal low prediction accuracies of the existing models, which are based on different conditions and simple linear equations. Additionally, the models with more reliable variables

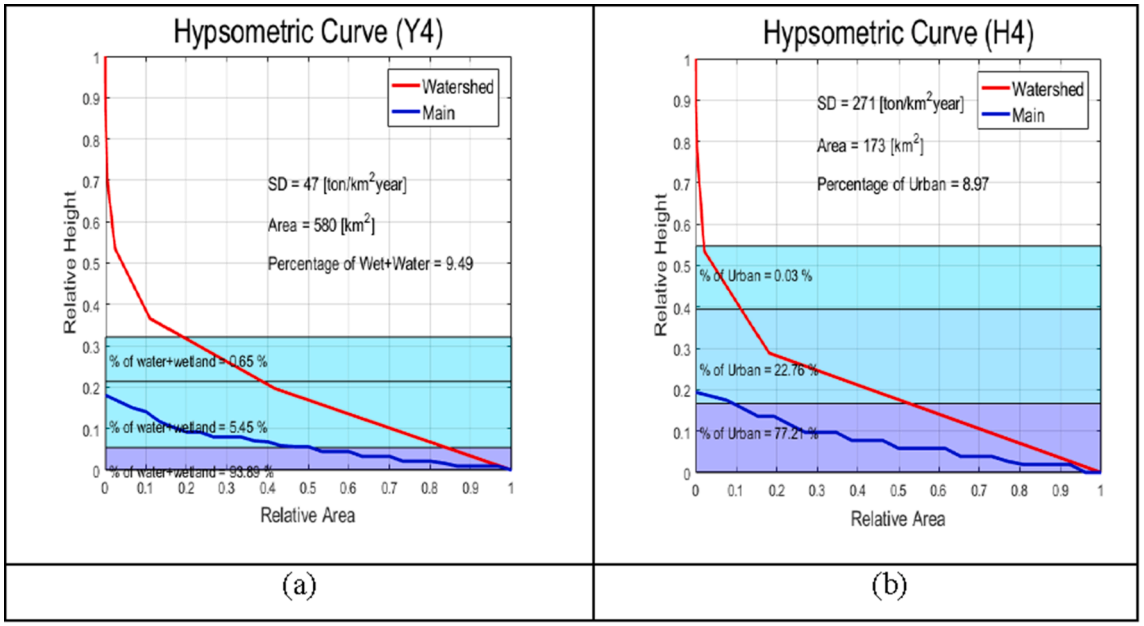

Fig. 9. Physiographical analyses (hypsometric curves) of stations Y4 and H4: (a) Y4, Nampyeong and (b) H4, Yulgeuk.

produce more reasonable results. The model developed with model tree and SEMEP provides the lowest RMSE (53 ton/km^2·yr) and highest NSE (0.48), which suggests good agreement between the model results and the measured specific degradation on these watersheds and the model well predicts the sediment yield than observed mean. The SEMEP-based model was found to produce better predictions for sand bed rivers with fine suspended materials. Yang and Julien (2019) also reported that SEMEP outperformed MEP, and their results were comparable with those of the present study.

4. Discussion

The statistical evaluation indicated that the existing models based on South Korea provide better predictability than the models based on other countries. Moreover, the data mining approach offers better accuracy than other methods. Conversely, it would be difficult to apply the model suggested in this study to other regions. However, this methodology could identify the important parameters affecting erosion and sediment. To evaluate the meaningful parameters of the proposed models, they were used to conduct geospatial analysis of upland erosion together with erosion maps with the revised soil loss equation (RUSLE), satellite images, and aerial photographs. Both models incorporate the elevation in the middle relative area determined from the hypsometric curve (*Hyp*) and the percentage of urban land (*U*). The results of the RUSLE for the urban land area at station N1 are shown in Fig. 6. The erosion map in Fig. 6 reveals that the urban land area is not a major erosional risk area (gross erosion of ~1 ton/km^2·yr). However, there are many regions with high annual soil erosion risks (>50 ton/ km^2·yr). The satellite image and aerial photograph reveal that most of these areas are construction sites, where the exposed soils are prone to erosion and large amounts of sediment can be easily transported into the river through surface runoff. In the case of the elevation in the middle relative area (*Hyp*), all the coefficients of determination were found to be negative. As shown in Fig. 7, the forested mountain regions are very far from the gauging stations. In addition, if the elevation in the middle relative area is low, the flat watershed would be more developed and provide a platform for sediment deposition. The MEP-based model incorporated the percentage of water and wetland. The erosion map of station N1 obtained by this model in Fig. 8 reveals many wetlands (brown) near alluvial rivers. Wetlands typically trap sediment during flood events and agricultural reservoirs are major locations of sediment deposition. The water areas, which are colored purple in Fig. 8b, occur along the rivers and in scattered agricultural reservoirs represented by the small purple dots. The 5-m-resolution erosion map properly captures two agricultural reservoirs, and the aerial photograph reveals flood plains near the alluvial rivers, with sand being the main formation material of the flood plains (Fig. 7b and d).

The mean annual precipitation in the SEMEP-based model is related to the raindrop impact and significantly supports the positive relationship between the specific degradation and precipitation (Lee and Heo, 2011). The proposed models incorporate two additional physical characteristics of the watershed, namely, the 1) mainstream length and 2) form factor. The mainstream length can be used as a meaningful parameter similar to the drainage area, because a longer mainstream increases the possibility of sedimentation. Similarly, the form factor can also be used as a meaningful parameter. In the case of the form factor, a lower value implies a higher peak flow over a shorter duration. This means that the sinuosity and a long travel time along an alluvial river are relevant to the specific degradation.

In the proposed models, the absolute value of the coefficient of determination for *WW* is the largest for a low elevation (M1 determined by MEP). From the result of physiographical analyses, more than 98% of the wetlands and waters were located below the middle relative area on the hypsometric curve for station Y4, which had the largest amount of water and wetland (*WW* = 9.49%). It suggests that upland erosion happens in the upstream part of the watersheds and sedimentation is observed on reservoirs and wetlands as the flood wave propagates downstream. The upland erosion in the urban lands also occurred in the lower part of the watershed (Fig. 9). However, the coefficient of determination for *U* was not dominant in M1 for both models. This is perhaps best explained by the fact that urban development is progressive in urbanized areas and spreads throughout the watershed.

Since the results of specific degradation do not show apparent differences and the data did not cover all watersheds in South Korea, additional research based on supplementary sediment measurement gauging stations in steep mountain watersheds could be helpful for improving the model's prediction accuracy for watersheds in South Korea. Moreover, the proposed models could be updated with extended survey periods. In terms of geospatial analysis, erosion maps at a higher resolution could clearly delineate high-risk erosion areas and provide detailed features.

5. Conclusion

The specific degradations estimated by MEP were within 10–1000 ton/km^2·yr, while those estimated by SEMEP were as much as 500 ton/km^2·yr, with most of the stations (25 out of 35) having specific degradations within 25% of each other. The results obtained by the two methods were respectively used in model tree analyses to develop empirical models. Existing statistical and regression models were also tested against the determined specific degradations. The predictabilities of the models were observed to depend on the type and characteristics of their catchments. The proposed SEMEP-based model was found to outperform all the other models (RMSE = 53 ton/km^2·yr and NSE = 0.48). The proposed MEP-based model utilizes the percentage of urban land, percentage of wetland and water, and elevation in the middle relative area. The meaningful parameters of the SEMEP-based model are the mean annual precipitation, percentage of urban land, and elevation in the middle relative area. The watershed morphometric variables (i.e., the mainstream length and form factor) also provide a classification standard. Further, the results of physiographical analyses based on hypsometric curves and geospatial analyses utilizing the RUSLE, satellite images, and aerial photographs revealed that wetland, water, and urban land were important indicators for predicting the specific degradation of watersheds. This prediction methodology could provide accurate prediction for the target area and can be useful for identifying watersheds, which require sustainable sediment management. Additionally, geospatial analysis using satellite images and aerial photographs enables evaluation of the prediction methodology. In conclusion, the sediment output (obtained by the SEMEP in this study) and the overall sediment budget of the catchment (the erosion map obtained by the RUSLE) considering the local conditions should both be incorporated in the development of a model of sediment transport and sediment yield.

Declaration of Competing Interest

The authors declare that they have no known competing financial interests or personal relationships that could have appeared to influence the work reported in this paper.

Acknowledgements

Funding: This work was supported by a grant (19AWMP-B121100-04) from the Advanced Water management Research program (AWMP) funded by the ministry of Land, infrastructure and Transport of Korean government.

References

Allen, P.B., 1986. Drainage density versus runoff and sediment yield. In: Fourth Federal Interagency Sedimentation Conference, LasVegas. USGS, pp. 3.

Aytek, A., Kişi, Ö., 2008. A genetic programming approach to suspended sediment modelling. J. Hydrol. 351 (3–4), 288–298.

Bhattacharya, B., Price, R., Solomatine, D., 2007. Machine learning approach to modeling sediment transport. J. Hydraul. Eng. 133 (4), 440–450.
Boix-Fayos, C., de Vente, J., Martínez-Mena, M., Barberá, G.G., Castillo, V., 2008. The impact of land use change and check-dams on catchment sediment yield. Hydrol. Process.: Int. J. 22 (25), 4922–4935. https://doi.org/10.1002/hyp.7115.
Chen, W., Xie, X., Wang, J., Pradhan, B., Hong, H., Bui, D.T., Ma, J., 2017. A comparative study of logistic model tree, random forest, and classification and regression tree models for spatial prediction of landslide susceptibility. Catena 151, 147–160.
Cobaner, M., Unal, B., Kisi, O., 2009. Suspended sediment concentration estimation by an adaptive neuro-fuzzy and neural network approaches using hydro-meteorological data. J. Hydrol. 367 (1–2), 52–61.
Colby, B.R., Hembree, C.H., 1955. Computations of total sediment discharge, Niobrara River near Cody, Nebraska. Water Supply Paper 1357. Washington, D.C., U. S. Geological Survey.
Ebtehaj, I., Bonakdari, H., Zaji, A.H., Azimi, H., Sharifi, A., 2015. Gene expression programming to predict the discharge coefficient in rectangular side weirs. Appl. Soft Comput. 35, 618–628.
Einstein, H.A., 1950. The bed-load function for sediment transportation in open channel flows. Technical Bulletin no. 1026. US Department of Agriculture, Washington, DC.
Esri, Arcgis for Desktop [Website] (2020. October 4). Retrieved from https://desktop.arcgis.com/en/arcmap/10.3/guide-books/extensions/geostatistical-analyst/fitting-a-model-to-the-empirical-semivariogram.htm.
Faran Ali, K., De Boer, D.H., 2008. Factors controlling specific sediment yield in the Upper Indus River basin, northern Pakistan. Hydrol. Process. 22 (16), 3102–3114. https://doi.org/10.1002/hyp.6896.
Gayen, A., Saha, S., Pourghasemi, H.R., 2019. Soil erosion assessment using RUSLE model and its validation by FR probability model. Geocarto Int. 1–19.
Ghani, A., Azamathulla, H.Md., 2011. Gene-expression programming for sediment transport in sewer pipe systems. J. Pipeline Syst. Eng. 2 (3), 102–106.
Holmquist-johnson, C. L. (2006). Bureau of Reclamation Automated Modified Einstein Procedure (BORAMEP) program for computing total sediment load.
Horton, R.E., 1932. Drainage-basin characteristics. EOS, Trans. Am. Geophys. Union 13 (1), 350–361.
Horton, R.E., 1945. Erosional development of streams and their drainage basins: hydro physical approach to quantitative morphology. Bull. Geol. Soc. Amer. 5, 275370.
Iovine, G., D'Ambrosio, D., Di Gregorio, S., 2005. Applying genetic algorithms for calibrating a hexagonal cellular automata model for the simulation of debris flows characterised by strong inertial effects. Geomorphology 66 (1–4), 287–303.
Jain, S.K., 2001. Development of integrated sediment rating curves using ANNs. J. Hydraul. Eng. 127 (1), 30–37.
Jang, E.K., 2017. Sediment Discharge Assessment for Rivers using Model Tree in Data Mining. Myongji University.
Julien, P.Y., 2010. River Mechanics. Cambridge University Press.
Kane, B., Julien, P., 2007. Specific degradation of watersheds. Int. J. Sedim. Res. 22 (2), 114–119.
Kang, W., 2019. Geospatial Analysis of Specific Degradation in SOUTH KOREA. 234 p. Dissertation.
Kang, W., Yang, C.Y., Lee, J., Julien, P.Y., 2019. Sediment yield for ungauged watersheds in South Korea. KSCE J. Civ. Eng. 23 (12), 5109–5120.
Kim, H.S., 2006. Soil erosion modeling using RUSLE and GIS on the Imha watershed, South Korea. M.S. Thesis, Colorado State University, Colorado, US.
Knox, J.C., 1977. Human impacts on Wisconsin stream channels. Ann. Assoc. Am. Geogr. 67 (3), 323–342. https://doi.org/10.1111/j.1467-8306.1977.tb01145.x.
Korea Institute of Civil Engineering and Building Technology (KICT), 1992. Research of sediment yield rate for dam design. Ministry of Transportation (in Korea).
Korea Institute of Civil Engineering and Building Technology (KICT), 2007. Surface water hydrological component analysis system development (in Korea), Research Report, 384. Ministry of Transportation. Sejong, KR: ME.
Langbein, W.B., 1947. Topographic characteristics of drainage basins. U.S. Geol. Survey, W.S. Paper 968-C, p. 125–155.
Langbein, W.B., Schumm, S.A., 1958. Yield of sediment in relation to mean annual precipitation. Eos, Trans. Am. Geophys. Union 39 (6), 1076–1084. https://doi.org/10.1029/TR039i006p01076.
Lee, J.H., Heo, J.H., 2011. Evaluation of estimation methods for rainfall erosivity based on annual precipitation in Korea. J. Hydrol. 409 (1), 30–48. https://doi.org/10.1016/j.jhydrol.2011.07.031.
Lee, J.H., Lee, J.H., Julien, P.Y., 2018. Global climate teleconnection with rainfall erosivity in South Korea. Catena 167, 28–43.
Lin, B., Namin, M.M., 2005. Modelling suspended sediment transport using an integrated numerical and ANNs model. J. Hydraul. Res. 43 (3), 302–310.
Merritt, W.S., Letcher, R.A., Jakeman, A.J., 2003. A review of erosion and sediment transport models. Environ. Modell. Software 18 (8), 761–799. https://doi.org/10.1016/S1364-8152(03)00078-1.
Minister of Environments (Me), 2002. Land Cover Map Using Artificial Satellite Image Data (in Korea). ME, Sejong, KR.
Minister of Environments (Me), 2012. Notification on investigation of soil erosion status (in Korea). ME, Sejong, KR.
Minister of Land, Transport and Maritime Affairs (MLTMA), 2011. Dam design manual and analysis, The Ministry of Land, Transport and Maritime Affairs (in Korea). ME, Sejong, KR.
Ministry of Construction (MOC), 1992. Research of specific sediment yield in watershed for dam design. Ministry of Construction, Korea.
Nagy, H., Watanabe, K., Hirano, M., 2002. Prediction of sediment load concentration in rivers using artificial neural network model. J. Hydraul. Eng. 128 (6), 588–595.
Ostovari, Y., Ghorbani-Dashtaki, S., Bahrami, H.A., Naderi, M., Dematte, J.A.M., Kerry, R., 2016. Modification of the USLE K factor for soil erodibility assessment on calcareous soils in Iran. Geomorphology 273, 385–395.
Özkaymak, Ç., Sözbilir, H., 2012. Tectonic geomorphology of the Spildağı high ranges, western Anatolia. Geomorphology 173, 128–140.
Ozturk, D., Kilic, F., 2016. Geostatistical approach for spatial interpolation of meteorological data. Anais da Academia Brasileira de Ciências 88 (4), 2121–2136.
Quinlan, J.R., 1992. Learning with continuous classes. In: 5th Australian Joint Conference on Artificial Intelligence. Singapore, pp. 343–348.
Renard, K.G., Foster, G.R., Weesies, G.A., McCool, D.K., Yoder, D.C., 1997. Predictingsoil erosion by water: a guide to conservation planning with the Revised Universal SoilLoss Equation (RUSLE), Vol. 703. United States Department of Agriculture, Washington, DC.
Rouse, H., 1937. Modern conceptions of the mechanics of fluid turbulence. Trans. ASCE 102, 463–505.
Ryu, H.J., Kim, S.W., 1976. Study on sedimentaion in reservoir. J. Hydrol. Sci., Korean Assoc. Hydrol. Sci. 9 (2), 67–75.
Ryu, S.C., Min, B.H., 1975. A Study for Sedimentation in Reservoir -on district of Chin Young-. Mag. Korean Soc. Agric. Eng., Korean Soc. Agric. Eng. 17 (3), 46–53.
Shah-Fairbank, S.C., 2009. Series expansion of the modified Einstein procedure. Colorado State University, Fort Collins, CO, p. 238. Dissertation.
Sheppard, J.R., 1965. Methods and their suitability for determining total sediment quantities. In: Proceedings of the Federal Inter-agency Sedimentation Conference 1963, U.S. Department of Agriculture, Agricultural Research Service, ed., Washington, D.C.
Shrestha, D.P., Zinck, J.A., Van Ranst, E., 2004. Modelling land degradation in the Nepalese Himalaya. Catena 57 (2), 135–156.
Shi, P., Zhang, Y., Ren, Z., Yu, Y., Li, P., Gong, J., 2019. Land-use changes and check dams reducing runoff and sediment yield on the Loess Plateau of China. Sci. Total Environ. 664, 984–994.
Singh, V.P., 1994. Elementary Hydrology. Hall of India Private Limited.
Strahler, A.N., 1952. Hypsometric (area-altitude curve) analysis of erosional topography. Bull. Geol. Soc. Am. 63 (11), 1117–1141. https://doi.org/10.1130/00167606(1952)63[1117:HAAOET]2.0.CO;2.
Van Remortel, R.D., Hamilton, M.E., Hickey, R.J., 2001. Estimating the LS factor for RUSLE through iterative slope length processing of digital elevation data within ArcInfo grid. Cartography 30 (1), 27–35.
Vente, J., Verduyn, R., Verstraeten, G., Vanmaercke, M., Poesen, J., 2011. Factors controlling sediment yield at the catchment scale in NW Mediterranean geoecosystems. J. Soils Sediments 11 (4), 690–707. https://doi.org/10.1007/s11368-011-0346-3.
Verstraeten, G., Poesen, J., 2001. Factors controlling sediment yield from small intensively cultivated catchments in a temperate humid climate. Geomorphology 40 (1), 123–144. https://doi.org/10.1016/S0169-555X(01)00040-X.
Viloria, J.A., Viloria-Botello, A., Pineda, M.C., Valera, A., 2016. Digital modelling of landscape and soil in a mountainous region: a neuro-fuzzy approach. Geomorphology 253, 99–207.
Wang, Y., Witten, I.H., 1996. Induction of model trees for predicting continuous classes. (Working paper 96/23). University of Waikato, Department of Computer Science, Hamilton, New Zealand.
Wheater, H., Jakeman, A., Beven, K., 1993. Progress and directions in rainfall-runoff modeling. Modeling Change in Environmental Systems, 101–132. Wiley.
Wessels, K.J., Prince, S.D., Malherbe, J., Small, J., Frost, P.E., VanZyl, D., 2007. Can human-induced land degradation be distinguished from the effects of rainfall variability? A case study in South Africa. J. Arid Environ. 68 (2), 271–297.
Williams, J.R., 1975. Sediment-yield prediction with universal equation using runoff energy factor. ARS-S-40. US Department of Agriculture, Agricultural Research Service, Brooksville, FL, pp. 244–252.
Wischmeier, W.H., Johnson, C., Cross, B., 1971. Soil erodibility nomograph for farmland and construction sites. J. Soil Water Conserv.
Woo, H.S., Kim, W., Ji, U., 2015. River hydraulics. CheongMoonGak publishing, Paju-Si, Korea.
Yang, C.Y., 2019. The sediment yield of South Korean Rivers. Colorado State University, Fort Collins, CO, p.238. Dissertation.
Yang, C.Y., Julien, P.Y., 2019. The ratio of measured to total sediment discharge. Int. J. Sedim. Res. 34 (3), 262–269.
Yoon, B., Woo, H., 2000. Sediment problems in Korea. J. Hydraul. Eng. 126 (7), 486–491. https://doi.org/10.1061/(asce)0733-9429(2000)126:7(486).
Yoon, Y.J., 2011. Devleopment of Prediction Formulae for Sediment Rate of Multipurpose Dams. Ph.D. Dissertation. Inha University, Incheon, Korea.
Zhu, Y.M., Lu, X.X., Zhou, Y., 2007. Suspended sediment flux modeling with artificial neural network: an example of the Longchuanjiang River in the Upper Yangtze Catchment, China. Geomorphology 84 (1–2), 111–125.